

Nanoscale

Accepted Manuscript



This is an *Accepted Manuscript*, which has been through the Royal Society of Chemistry peer review process and has been accepted for publication.

Accepted Manuscripts are published online shortly after acceptance, before technical editing, formatting and proof reading. Using this free service, authors can make their results available to the community, in citable form, before we publish the edited article. We will replace this *Accepted Manuscript* with the edited and formatted *Advance Article* as soon as it is available.

You can find more information about *Accepted Manuscripts* in the [Information for Authors](#).

Please note that technical editing may introduce minor changes to the text and/or graphics, which may alter content. The journal's standard [Terms & Conditions](#) and the [Ethical guidelines](#) still apply. In no event shall the Royal Society of Chemistry be held responsible for any errors or omissions in this *Accepted Manuscript* or any consequences arising from the use of any information it contains.

Cite this: DOI: 10.1039/c0xx00000x

www.rsc.org/xxxxxx

PAPER

Aspect ratio effect of drug nanocrystals on cellular internalization efficiencies, uptake mechanisms, *in vitro* and *in vivo* anticancer efficiencies†

Baishun Tian, Xiujuan Zhang*, Caitong Yu, Mengjiao Zhou and Xiaohong Zhang*

5 Received (in XXX, XXX) Xth XXXXXXXXX 20XX, Accepted Xth XXXXXXXXX 20XX

DOI: 10.1039/b000000x

In this paper, we investigated the aspect ratio (AR) effect of anticancer drug nanocrystals (NCs) on their cellular internalization efficiency, uptake mechanisms, biodistributions as well as *in vitro* and *in vivo* antitumor efficiencies. Both confocal image and flow cytometry show that shorter NCs with AR=1 have 10 much faster cellular uptake rate and much higher anticancer efficacy than that of longer NCs. All NCs with different ARs were found to enter the cells via energy-dependent clathrin-mediated pathway. *In vivo* experiments indicate that NCs with higher ARs have shorter half-life and are more easily captured by liver, while the corresponding tumor uptake decreased. We also observed that NCs with the smallest AR have the highest therapeutic efficacy with appreciable less weight loss. These results would assist in the 15 future design of drug NCs and may lead to the development of new drug nanostructures for biomedical applications.

Introduction

Cancer remains one of the most devastating diseases and chemotherapy has become an indispensable mode of treatment 20 for malignant tumors. Recent development of nanobiotechnology provides new hopes for cancer therapy, several nanoenabled drug delivery systems have gained applications in the pharmaceutical industry.¹⁻⁶ Among them, nanonization of drugs into nanocrystals (NCs) has become very promising, because compared with other 25 formulations, drug NCs can not only improve the solubility, dissolution kinetics and bioavailability of drugs, but also they have the minimal use of excipients, which implies both high drug loading content and diminished excipient-related toxicity.⁷⁻¹⁷ Their very high drug loading capacity will lead to higher 30 deposition of drugs selectively at the tumor sites via the leaky vessels by the enhanced permeability and retention (EPR) effect.¹² To date, some drug NCs have been clinically approved or are under clinical investigations.^{13,14}

Recent observation shows that non-spherical drug NCs with a 35 high aspect ratio (AR) exhibit better pharmacokinetics and efficiency in drug delivery than spherical ones, due to their enhanced internalization rates, multiple endocytic mechanisms, and more effective adhesion to the target cell surface.¹⁵ But how exactly the AR will affect the biological outcomes like the rate of 40 cellular uptake, the mechanism of uptake, biodistribution and biocompatibility, is unknown. In this regards, some studies have demonstrated that internalization of cylindrical particles depends strongly on their aspect ratio. Particles with an aspect ratio of three were internalized about four times as fast as their spherical 45 counterparts of the same volume.¹⁶ However, other studies show that the uptake of gold nanoparticles by receptor-mediated endocytosis significantly decreased with increased aspect ratios.¹⁷ Therefore, the AR effect varies according to different systems.

Herein in this paper, we investigated the aspect ratio effect of 50 anticancer drug NCs on their cellular internalizing efficiency, the uptake mechanisms, biodistributions as well as *in vitro* and *in vivo*

in vivo antitumor efficiencies. These results would assist in the future design of drug nanocrystals and may lead to the development of new drug nanostructures for biomedical 55 applications.

Results and Discussion

Design of PEGylated 10-HydroxyCamptothecin (HCPT) NCs with Different ARs

In order to probe the influence of AR of drug NCs on cellular 60 uptake, *in vitro* and *in vivo* anticancer activities, HCPT NCs with different ARs were prepared by using a solvent exchanging method and designated as HCPT-1, HCPT-2, HCPT-3 and HCPT-4.¹⁸ The dimension were measured and analyzed by the scanning electron microscopy (SEM) images (Fig. 1a-d). The 65 mean ARs of HCPT-1, HCPT-2, HCPT-3 and HCPT-4 are about 1.3, 2.0, 3.2 and 4.0, respectively.

We then make surface functionalization of HCPT NCs by [poly(maleic anhydride-alt-1-octadecene)-polyethylene glycol (C18PMH-PEG)] through noncovalent hydrophobic interaction to 70 achieve good water-dispersibility and bio-environmental stability.¹⁹ It should be noted that modified HCPT NCs preserve very stable size (Fig. 1e) in physiological saline even over 3 days. In a striking contrast, non-functionalized HCPT NCs show continuous size increase, due to elimination of the surface charge 75 by zwitterions in physiological saline. Thus, it shows that surface modification of HCPT NCs was successfully achieved. We further examined drug release profile of the functionalized HCPT NCs as shown in Fig. 1f. Compared with the longer NCs (HCPT-4), the shorter NCs (HCPT-1) exhibited relatively faster release. 80 A possible explanation could be that shorter NCs possess much

larger surface areas than the longer ones, which induces relatively faster drug release.

Cellular Uptake of HCPT NCs with different ARs

In order to assess cellular uptake of different ARs of HCPT NCs in human nasopharyngeal epidermal carcinoma (KB) cell line, we

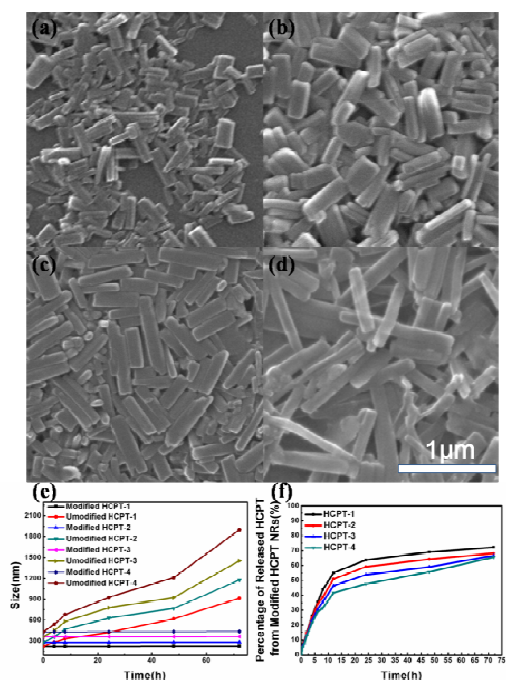


Fig. 1 (a-d) SEM images of the HCPT NCs with different ARs. (e) Stability studies of modified HCPT NCs and unmodified HCPT NCs in physiological saline. (f) Time-dependent release of HCPT from PEGylated HCPT NCs in a PBS solution (pH 7.4) at 37 °C for 24 h, data were obtained by measuring the fluorescence intensity of free HCPT in solution ($\lambda_{em} = 550$ nm; $\lambda_{ex} = 382$ nm).

used a combination of confocal laser-scanning fluorescent microscopy (CLSM) and flow cytometry assay. Confocal images were obtained for all incubated cells based on the fluorescence of HCPT and DCJTb (a red fluorescent dye with high quantum yield, which was encapsulated in HCPT NCs for labelling). KB cells were incubated with PEGylated HCPT NCs ([HCPT] = 12 μ M) for 4 and 8 h at 37 °C and then washed by phosphate buffered saline (PBS) buffer before confocal imaging. As shown in Fig. 2a and 2b, at the same incubation time, more intense fluorescence could be detected from the KB cells exposed to HCPT-1 than that from other groups (HCPT-2, HCPT-3, HCPT-4), implying much higher cellular uptake of HCPT-1 than other groups. This validated that cellular internalization of HCPT NCs exhibited strong AR dependent effect. A possible explanation for this behaviour could be that shorter NCs possess much larger surface areas in contact with the cell membrane than those of longer ones.²⁰ To further confirm that the cellular internalization rate was dependent on AR of NCs, the amount of internalized particles in KB cells was evaluated by flow cytometry. As shown in Fig. 2c and 2d, the shorter the NCs is, the larger amount of internalized particles in KB cells are detected, which is well consistent with the confocal imaging results.

The cellular uptake mechanism of the HCPT NCs with

different ARs was further investigated. Cells were first pre-incubated at low temperature (4 °C) and then treated with HCPT NCs with different ARs to minimize the active cellular processes, a marked decrease in the cellular internalization of all particles were observed (above 85 % compared with non-treated cells), indicating that internalization is an energy-dependent process.

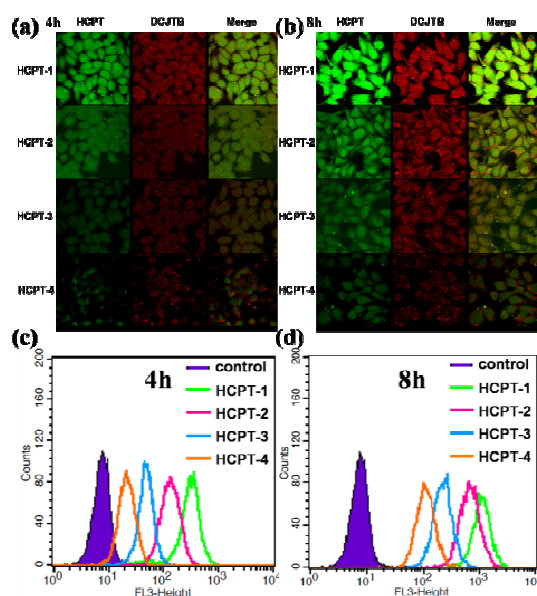


Fig. 2 (a, b) CLSM images of KB cells incubated with DCJTb@HCPT NCs with different ARs ([HCPT] = 12 μ M) for 4 and 8 h at 37 °C. (c, d) Fluorescent intensity of DCJTb in KB cells incubated with DCJTb@HCPT NCs with different ARs analyzed by FACS for 4 and 8 h at 37 °C.

Then the KB cells were treated with known biochemical inhibitors of clathrin-mediated endocytosis, caveolae-mediated endocytosis, and macropinocytosis. As shown in Fig. 3, barely any signal was noted for KB cells incubated with chlorpromazine and at 4 °C, while the fluorescence from other groups was not reduced, indicating that all NCs enter cells primarily by the energy-dependent clathrin-mediated pathway.

In Vitro Anticancer Efficacy of HCPT NCs with Different ARs

We also studied the effect of HCPT NCs with different ARs on cell viability. Measurements were carried out with KB cells and murine 4T1 breast cancer cell line (4T1 cells) incubated with HCPT NCs at a series of concentrations for 24, 48 and 72 h. The cytotoxicity was evaluated by using a traditional 3-(4,5-dimethylthiazol-2-yl)-2,5-diphenyltetrazolium bromide (MTT) assay. The time- and dose-dependent toxicity shown in Fig. 4 revealed that HCPT-1 reduced more strongly the metabolic activity of KB cells and 4T1 cells than other HCPT NCs at the same concentrations and for all exposure times, indicating that the cytotoxicity of the HCPT NCs is AR-dependent. The improved drug efficiency of shorter NCs should be benefit from the more effective cellular internalization for HCPT-1 than that of longer NCs. In turn, the cytotoxicity studies of HCPT NCs with different ARs can also provide evidence to support the fact that shorter NCs could transverse the cell membrane more easily.²¹

In Vivo Blood Circulation and Biodistribution of HCPT NCs

To verify the applicability of the HCPT NCs for *in vivo* drug delivery and investigate the *in vivo* pharmacokinetics, we injected PEGylated HCPT NCs via tail vein into Balb/c mice and studied HCPT levels in the blood over time. Blood was drawn at different

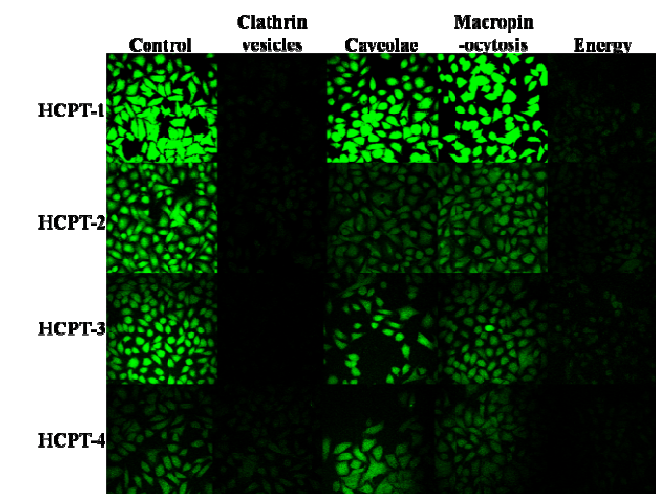


Fig. 3 CLSM images of KB cells incubated with chlorpromazine (10 µg/mL) to inhibit the formation of clathrin vesicles, filipin III (1 µg/mL) to inhibit caveolae, amiloride (50 µM) to inhibit macropinocytosis and at 4 °C to inhibit energy, and then incubated with PEGylated HCPT NCs with different ARs ([HCPT] = 12 µM) for 4 h.

measured blood fluorescence intensity). As shown in Fig. 5a, the half-life blood circulation times were about 2.6, 2.5, 2.1 and 1.9 h for HCPT-1, HCPT-2, HCPT-3 and HCPT-4, respectively. The long circulation time in the bloodstream allows repeated passes of nanomaterials through tumor blood vasculatures and is favorable for passive tumor targeting via EPR effect.

We next investigated the *in vivo* biodistribution of PEGylated HCPT NCs. 4T1 tumor-bearing Balb/c mice intravenously injected with PEGylated HCPT NCs were sacrificed at 1, 2, 6, 12, 24 and 48 h post-injection. The major organs of the mice (n = 3 per group) were weighed and solubilized by a lysis buffer for HCPT extraction. The concentration of HCPT in each organ was measured by fluorescence intensity.²³ Organs from a control mouse without injection of NCs were collected and used as controls to subtract the auto fluorescence background in various tissues. High levels of all lengthed NCs were observed in the tumor sites as well as reticuloendothelial systems (RES) organs such as liver, spleen and lung after 12 h circulation (Fig. 5b). The high tumor accumulation could be due to the effective EPR effect in cancerous tumors with tortuous and leaky vasculatures. It should be noted that the liver uptake became larger with the increased ARs, while the tumor uptake decreased accordingly. This phenomenon suggested that NCs with higher ARs were more easily captured by liver and also reflected the role of liver as the main clearance route for the NCs.

In Vivo Therapeutic Efficacy of HCPT NCs with Different ARs

Motivated by the high tumor accumulation of the NCs, we then

investigated the *in vivo* therapeutic efficacy of HCPT NCs by using the 4T1 tumor model on Balb/c mice. Tumor-bearing mice were randomly divided into six groups (n = 7): (1) a PBS vehicle control; (2) a HCPT control dissolved in a 7.5% (v/v) of excipient mixture and PBS (200 µL of 1 mg/mL per mouse, or a dose of 10 mg/kg); (3) PEGylated HCPT-1 (10 mg/kg HCPT-equivalent dose); (4) PEGylated HCPT-2 (10 mg/kg HCPT-equivalent dose); (5) PEGylated HCPT-3 (10 mg/kg HCPT-equivalent dose); (6) PEGylated HCPT-4 (10 mg/kg HCPT-equivalent dose).

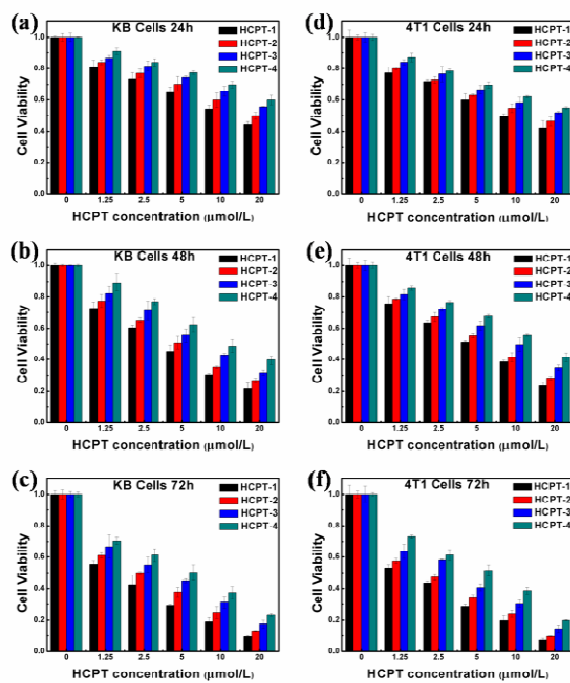


Fig. 4 MTT assay of HCPT NCs with different ARs at different concentrations and exposed times against KB cells (a-c) and 4T1 cells (d-f)

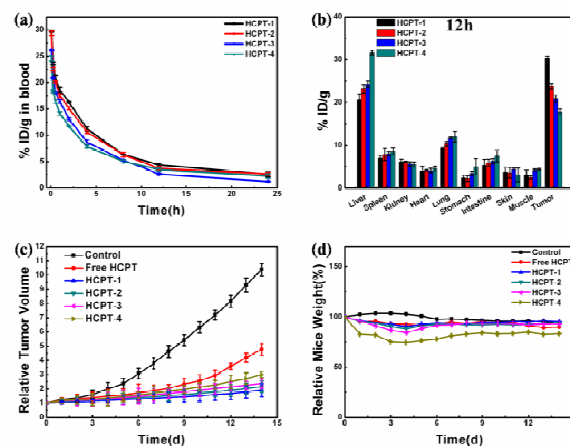


Fig. 5 (a) Blood circulation curve of HCPT NCs with different ARs after intravenous injection as determined by measuring HCPT fluorescence in the blood at different time points post-injection. The unit is percentage of injected dose per gram tissue (% ID/g). (b) Biodistribution of HCPT NCs with different ARs in mice after incubated in 12 h determined by the HCPT fluorescence. (c) Growth of 4T1 tumors in different groups of mice after treatment and (d) weights in different groups of mice after treatment.

The treatment was administered once per week through tail vein injection and lasted for 2 weeks. The mice were observed daily for clinical symptoms and the tumor size were measured by a caliper every day after treatment. The tumor growth rates were compared between the six groups over time using a random-effects mixed model including an interaction.²⁴ As shown in Fig. 5c, the tumors in PBS treatment rapidly increased by 10.37 ± 0.41 fold. The HCPT-1, HCPT-2, HCPT-3, and HCPT-4 (10 mg/kg) treated groups showed a greater antitumor effect compared to the HCPT in the excipient mixture at the equivalent dose (1.91 ± 0.46 , 2.16 ± 0.40 , 2.36 ± 0.33 , 3.01 ± 0.21 and 4.77 ± 0.41 fold tumor growth, respectively). NCs with the smallest AR have the highest antitumor efficacy than other groups. Body weights of animals were also daily monitored (Fig. 5d). Compared with the control group, animals receiving free HCPT and PEGylated HCPT NCs administration both showed a cyclical decrease in body weight following each of the weekly drug administration. Free HCPT exhibited a little lower weight loss than that of HCPT NCs. Moreover, the weight loss became more obvious with the increase of AR for HCPT NCs. This suggested that the toxic side effect of HCPT NCs with larger ARs was much higher than the other groups, which may be due to their larger accumulation in liver and tardy metabolism by mice. However, after 2 weeks, the body weight recovered to the original level before administration in any of the treatment groups except HCPT-4 group, indicating a negligible acute toxicity of HCPT NCs with smaller AR at this dose (10 mg/kg HCPT-equivalent).

Conclusion

In summary, HCPT NCs with four different ARs were controllably developed, which exhibited a strong AR dependent cellular internalizing efficiency, *in vitro* and *in vivo* anticancer efficiency. Shorter HCPT NCs showed obviously enhanced internalization rates than that of longer NCs, which maybe benefit from the fact that shorter NCs possess much larger surface areas in contact with the cell membrane than that of longer ones. *In vivo* experiments show that NCs with higher ARs have shorter half-life and are more easily captured by liver, while NCs with the smallest AR possess the highest therapeutic efficacy with appreciable less weight loss. These results would assist in the future design of drug nanocrystals in bioapplications.

Experimental section

Materials and Measurements

HCPT was purchased from Knowshine (Shanghai, China), and ethanol from Sinopharm Chemical Reagent Co. (China). Fetal bovine serum (FBS), Roswell Park Memorial Institute-1640 (RPMI-1640) medium, and Penicillin-streptomycin solution were purchased from Invitrogen (San Diego, CA). MTT was purchased from Sigma Aldrich (Milwaukee, WI). Distilled water was obtained from a Milli-Q Biocel water purification system ($18.2 \text{ M}\Omega\cdot\text{cm}$ resistivity) (Millipore Corporation, Bedford, USA). KB cells were provided by American Type Culture Collection(ATCC). Unless otherwise noted, all the chemicals were obtained from commercial suppliers and used without further purification. UV-vis absorption spectra were obtained on a Perkin-Elmer Lambda 750 UV/vis/NIR absorbance

spectroscopy. The fluorescence spectra were obtained from a FluoroMax 4 (Horiba Jobin Yvon) spectrofluorimeter. SEM images were obtained on a FEI Quanta 200 FEG field emission scanning electron microscope operated at an accelerating voltage of 30 kV.

Preparation and PEGylated of HCPT NCs

The NCs was synthesized by a previously published protocol.¹⁵ In detail, 500 μL of $1 \times 10^{-3} \text{ M}$ HCPT/ethanol solution was dropped into 10 mL of aqueous solution at room temperature under rapid stirring. NCs with length about 1-2 μm were obtained, and then they were further applied sonication treatment with different time courses (2, 5, 12, and 24 h) for the formation of NCs with different ARs (HCPT-1, HCPT-2, HCPT-3, HCPT-4). For surface modification of NCs, C18PMH-PEG was first synthesized following a literature procedure,²⁵ 1mg C18PMH-PEG was then dispersed in 10 mL distilled water, and 300 μL solutions was added into 5 mL stock solution of HCPT NCs. The mixture was treated with sonication for 5 min.

Characterization Measurements

The size of the NCs was measured by DLS at 25 °C. The mean value of each sample was obtained from at least 20 times measurements. The morphology and particle size were further characterized by SEM. Samples for SEM observation were prepared by dropping some suspension of NCs onto silicon substrates, then 2 nm layer of Au was deposited on it after solvent evaporation.

HCPT Release Assay from PEGylated HCPT NCs

PEGylated HCPT NCs suspensions (2 mL) were added into a dialysis bag (MWCO 5000) and immersed into 50 mL of PBS at 37 °C with stirring for drug release. Aliquots of 2 mL were at a predetermined time withdrawn from the solution to containers. The solution volume was kept constant by adding 2 mL fresh PBS after each sampling. The amount of HCPT released was determined by using fluorescence measurement (excitation at 382 nm).

Cell Culture

KB and 4T1 cells were grown in normal RPMI-1640 culture medium supplemented with 10% fetal bovine serum (FBS) and 1% penicillin/streptomycin solution at 37 °C in a humidified atmosphere containing 5% CO₂. Cells were routinely passaged by treatment with trypsin (0.05%)/EDTA.

Confocal Imaging of Cells

Confocal imaging of cells was performed using a Leica laser scanning confocal microscope. Imaging of HCPT was carried out under 405 nm laser excitation and emission was collected in the range of 500 to 600 nm. KB cells were incubated with PEGylated HCPT NCs ([HCPT] = 12 μM) for 4 and 8 h before confocal imaging. All cells were washed twice with PBS buffer before confocal imaging.

Cellular Uptake Measured by Flow Cytometry

KB cells were seeded in 24-well plates (1 mL/well). The plates were then incubated at 37 °C for 24 h in a humidified atmosphere containing 5% CO₂. The cells were then incubated with

PEGylated HCPT NCs. The drug-treated cells were incubated for pre-determined time at 37 °C, and then washed twice with cold PBS, and digested by trypsin (0.05%)/EDTA treatment. The suspensions were centrifuged at 1000 rpm and 4 °C for 4 min.

The supernatants were discarded and the cell pellets were washed with PBS to remove the background fluorescence in the medium. After two cycles of washing and centrifugation, cells were resuspended with 1 mL PBS and disrupted by vigorous sonication. The amount of HCPT in sonicated mixture was analyzed by using flow cytometry assay. Blank cells sample without drug nanocrystals injection was measured as control.

Cytotoxicity Assays

The *in vitro* cytotoxicity was measured by using a standard MTT assay. KB and 4T1 cells were seeded into 96-well plates (100 µL/well). The plates were then incubated at 37 °C for 24 h in a humidified atmosphere containing 5% CO₂. Cells were then treated with various concentrations of HCPT NCs. The drug-treated cells were incubated at 37 °C for pre-determined time in a humidified atmosphere containing 5% CO₂. The cells were then treated with 20 µL of MTT solution (5 mg/mL in PBS) and incubated for 5 h. The medium was removed and the cells were lysed by adding 150 µL of DMSO, the cell viabilities were then measured by MTT assay and the relative cell survival percentages compared to the drug-free control were plotted against the drug concentration in logarithmic scale.

Tumor Models

4T1 murine breast cancer cells were cultured in RPMI-1640 supplemented with 10% FBS and 1% penicillin-streptomycin. Balb/c mice were obtained from Nanjing Peng Sheng Biological Technology Co, Ltd and performed under protocols approved by Soochow University Laboratory Animal Center. The 4T1 tumor models were generated by subcutaneous injection of 2 × 10⁶ cells in 60 µL PBS into the right shoulder of female Balb/c mice. The mice were used for treatment when the tumor volume reached 50-100 mm³ (~6 days after tumor inoculation).

Blood Circulation

Blood circulation was measured by drawing ~10 µL blood from the tail vein of Balb/c mice post injection of PEGylated HCPT NCs. Each blood sample was dissolved in 1 mL of lysis buffer (1% SDS, 1% Triton X-100, 40 mM Tris Acetate). The concentration of PEGylated HCPT NCs in the blood was determined by the fluorescence spectrum of each solubilized blood sample using a FluoroMax 4 fluorometer. A series of dilutions of the PEGylated HCPT NCs suspensions were measured to obtain a standard calibration curve. Blank blood sample without PEGylated HCPT NCs injection was measured to determine the blood auto-fluorescence level, which was subtracted from the fluorescence intensities of injected samples during the concentration calculation.

Biodistribution Measurement

For biodistribution study, 4T1 tumor-bearing mice (tumor size ~100 mm³) were sacrificed at 1, 2, 6, 12 and 24 h post injection of PEGylated HCPT NCs. The organs/tissues were weighed and homogenized in the lysis buffer (the same as the above used in the blood circulation experiment) with a PowerGen homogenizer

(Fisher Scientific). Clear homogeneous tissue solutions were obtained and diluted 10-100 times to avoid significant light scattering and self-quenching during fluorescence measurement. The fluorescence intensities of both standard samples and real tissue samples were all adjusted to be in the linear range by appropriate dilution. The sample was measured in triplicate to ensure reproducibility and measurement accuracy. The biodistribution of PEGylated HCPT NCs in various organs of the mice was then calculated and plotted in units of %ID/g.

In Vivo Therapeutic Antitumor Efficacy

For the treatment, 4T1 tumor-bearing mice were divided into six groups (n = 7) in a way to minimize weight and tumor size differences among the groups: (1) PBS vehicle (the control group), (2) HCPT excipient at 10 mg/kg; (3) PEGylated HCPT-1; (4) PEGylated HCPT-2; (5) PEGylated HCPT-3; (6) PEGylated HCPT-4 (10 mg/kg HCPT-equivalent dose). When the tumor volume reached 50-100 mm³, therapy was continued through tail vein injection for two weeks. The tumor sizes were measured by a caliper every the other day and tumor volumes were calculated as $a \times b^2/2$, where a was the largest and b the smallest diameter. Relative tumor volumes were calculated as V/V_0 (V_0 was the tumor volume when the treatment was initiated). Body weights of animals were also daily monitored. Mice were weighed with the relative body weights normalized to their initial weights.

Acknowledgement

This work was supported by National Natural Science Foundation of China (Nos. 51173124, 51172151), National Basic Research Program of China (973 Program, Grant Nos. 2013CB933500, 2012CB932400). We also thank a Project Funded by the Priority Academic Program Development of Jiangsu Higher Education Institutions.

Notes and references

- Functional Nano & Soft Materials Laboratory (FUNSOM) and Collaborative Innovation Center of Suzhou Nano Science and Technology Jiangsu Key Laboratory for Carbon-Based Functional Materials & Devices, Soochow University, Suzhou, Jiangsu 215123, China. E-mail: xjzhang@suda.edu.cn, xiaohong_zhang@suda.edu.cn; Tel: +86 512 65880955*
- † Electronic Supplementary Information (ESI) available. See DOI: 10.1039/b000000x/
- M. J. Sailor, J.H. Park, *Adv. Mater.*, 2012, **24**, 3779–3802.
 - L. F. Zhang, J. M. Chan, F. X. Gu, J.W.Rhee, A. Z. Wang, A. F. Radovic-Moreno, F. Alexis, R. Langer and O. C. Farokhzad, *ACS Nano*, 2008, **2**, 1696-1702.
 - Y. Wang, R. Guo, X. Y. Cao, M. W. Shen and X. Y. Shi, *Biomaterials*, 2011, **32**, 3322-3329.
 - T. Y. Jiang, R. Mo, A. Bellotti, J. P. Zhou and Z. Gu, *Adv. Funct. Mater.*, 2014, **24**, 2295–2304.
 - R. N. Majzoub, C.L. Chan, K. K. Ewert, Br. F. B. Silva, K. S. Liang, E. L. Jacovetty, B. Carragher, C. S. Potter and C. R. Safinya, *Biomaterials*, 2014, **35**, 4996-5005.
 - E. Yuba, A. Harada, Y. Sakanishi, S. Watarai, K. Kono, *Biomaterials*, 2013, **12**, 3042-3052.
 - K. Baba, H. E. Pudavar, I. Roy, T. Y. Ohulchanskyy, Y. Chen, R. K. Pandey and P. N. Prasad, *Mol. Pharm.*, 2007, **4**, 289-297.
 - A. Agarwal, Y. Lvov, R. Sawant and V. Torchilin. *J. Controlled Release*, 2008, **128**, 255-260.

- 9 F. Liu, J. Y. Park, Y. Zhang, C. Conwell, Y. Liu, S. R. Bathula and L. Huang, *J. Pharm. Sci.*, 2010, **99**, 3542-3551.
- 10 W. Li, Y. L. Yang, C. Wang, X. J. Zhang, F. F. An, X. J. Diao, X. J. Hao and X. H. Zhang, *Chem. Commun.*, 2012, **48**, 8120-8122.
- 5 11 M. J. Zhou, X. J. Zhang, Y. Y. Yang, Z. Liu, B. S. Tian, J. J. Jie and X. H. Zhang, *Biomaterials*, 2013, **34**, 8960-8967.
- 12 Y. Matsumura and H. Maeda, *Cancer Res.*, 1986, **46**, 6387-6392.
- 13 E. Merisko-Liversidge, P. Sarpotdar, J. Bruno, S. Hajj, L. Wei, N. Peltier, J. Rake, J. M. Shaw, S. Pugh, L. Polin, J. Jones, T. Corbett, E. Cooper and G. G. Liversidge, *Pharm. Res.*, 1996, **13**, 272-278.
- 10 14 J. J-UA and M. RH, *Int. J. Nanomedicine*, 2008, **3**, 295-309.
- 15 15 W. Li, X. J. Zhang, X. J. Hao, J. S. Jie, B. S. Tian and X. H. Zhang, *Chem. Commun.*, 2013, **49**, 10989-10991.
- 16 S. E. A. Gratton, P. A. Ropp, P. D. Pohlhaus, J. C. Luft, V. J. Madden, M. E. Napier and J. M. DeSimone, *Proc. Natl. Acad. Sci. U.S.A.*, 2008, **105**, 11613-11618.
- 17 B. D. Chithran, A. A. Ghazani, and W. C. W. Chan, *Nano Lett.*, 2006, **6**, 662-668.
- 18 X. Zhang, C. Dong, J. A. Zapien, S. Ismathullakhan, Z. Kang, J. Jie, X. Zhang, J. C. Chang, C. S. Lee and S. T. Lee, *Angew. Chem. Int. Ed.*, 2009, **48**, 9121-9123.
- 19 K. Knop, R. Hoogenboom, D. Fischer and U. S. Schubert, *Angew. Chem. Int. Ed.*, 2010, **49**, 6288-6308.
- 20 V. P. Chauhan, Z. Popović, O. Chen, J. Cui, D. Fukumura, M. G. Bawendi and R. K. Jain, *Angew. Chem. Int. Ed.*, 2011, **50**, 11417-11420.
- 21 L. Horváth, A. Magrez, D. Golberg, C. Zhi, Y. Bando, R. Smajda, E. Horváth, L. Forró and B. Schwaller, *ACS Nano*, 2011, **5**, 3800-3810.
- 22 Y. Matsumura and H. Maeda, *Cancer Res.*, 1986, **46**, 6387-6392; H. Maeda, J. Wu, T. Sawa, Y. Matsumura and K. Hori, *J. Controlled Release*, 2000, **65**, 271-284.
- 23 Z. Liu, A. C. Fan, K. Rakhra, S. Sherlock, A. Goodwin, X. Chen, Q. Yang, D. W. Felsher and H. Dai, *Angew. Chem. Int. Ed.*, 2009, **48**, 7668-7672; X. Zhang and B. Chen, *Cancer Lett.*, 2010, **298**, 26-33.
- 30 24 R. C. Littell, P. R. Henry and C. B. Ammerman, *J. Anim. Sci.*, 1998, **76**, 1216-1231.
- 25 Y. L. Yang, F. F. An, Z. Liu, X. J. Zhang, M. J. Zhou, W. Li, X. J. Hao, C. S. Lee, X. H. Zhang, *Biomaterials*, 2012, **33**, 7803-7809.

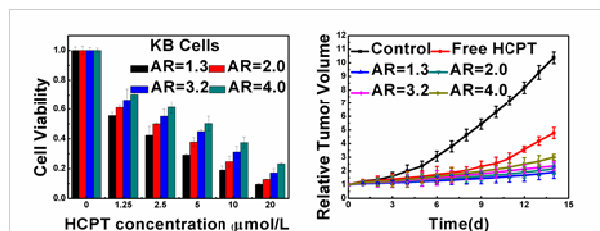
40

Cite this: DOI: 10.1039/c0xx00000x

www.rsc.org/xxxxxx

PAPER

Table of Contents



Aspect ratio effect of drug nanocrystals on their in vitro cellular internalizing efficiency and in vivo antitumor efficiencies was investigated.